metals

Sheet Metal forming optimization methodology for servo presses process control improvement

Antonio Del Prete [1], Teresa Primo [2,*]

[1] Department of Engineering for Innovation, University of Salento, Via per Arnesano, Building "O", 73100, Lecce, Italy; antonio.delprete@unisalento.it
[2] Department of Engineering for Innovation, University of Salento, Via per Arnesano, Building "O", 73100, Lecce, Italy; teresa.primo@unisalento.it
* Correspondence: teresa.primo@unisalento.it;

Received: date; Accepted: date; Published: date

Abstract: In sheet metal forming manufacturing operations the use of servo presses is gaining more and more interest thanks to the given opportunity to improve process performance (quality, productivity, cost reduction, etc.). It is not yet clear how to proceed in the engineering process when this type of operating machines is used to take the maximum possible advantage. Recently, several press builders developed gap and straight-sided metal forming presses adopting the mechanical servo-drive technology. The mechanical servo-drive press offers the flexibility of a hydraulic press with the: speed, accuracy and reliability of a mechanical press. Servo drive presses give the opportunity to improve: process conditions productivity and the stamped parts quality. Forming simulation and numerical optimization can be useful tools to define, preventively, what is the optimal process parameters set up in terms of servo press downward curve properties, owing to the possibility to carry out, preventively, a sensitivity analysis of the forming parameters having influence on said curve. The authors have developed a numerical methodology able to analyze the influence factors, for comparison with the degrees of freedom made available by the usage of a servo press, in terms of stroke profile management, to obtain an optimized process parameters combination.

Keywords: servo press, metal forming, automotive, optimization;

Introduction

Electro-mechanical servo-drives have been used in machine tools for several decades. Recently, several press builders, mainly in Japan [1], [2] and Germany [3], developed metal forming presses able to utilize the mechanical servo-drive technology. The mechanical servo-drive press offers the flexibility of a hydraulic press (infinite sliding – ram – speed and position control, availability of press force at any slide position) with the: speed, accuracy and reliability of a mechanical press [4]. The advantage of the servo motor is that it can control all the press motion such as speed, stroke, slide motion and position, therefore for the mechanical servo press flywheel, clutch and brake are replaced by high-capacity motors, and thus the maintenance of the servo press is simplified. Compared with traditional presses that have been used for many years, the mechanical servo press allows to obtain higher productivity, better product quality, simpler set up and maintenance, and high repeatability. One of the most important advantages of the servo press is the flexible slide movement [5]. As discussed above, the following quality are considered to be brought about by choosing a motion suitable for each aim.

1. The accumulated know-hows with the existing presses can be inherited because the motions such as crank press and linkage press can be duplicated by a servo press.
2. Impact loading is avoided and the tools life is extended by reducing the contact speed when the tool hits the blank.

3. Lubrication is often improved and the working limit can be extended by using a pulsating or oscillating slide motion.
4. Contact and break-through noise is reduced by stopping the slide for a short time or reducing the slide speed.
5. Blank vibration can be reduced by an optimized slide motion and the shape of sheet metal product is stabilized.
6. The product quality can be improved by controlling the slide parallelism and choosing an optimum slide motion.
7. Higher productivity is possible by shortening of a forming cycle with a partial short stroke around bottom dead center as well as a high speed return motion.

Wrinkles represent one of the most frequent defects during deep drawing processes that should be avoided and the function of the blank holder force is proper to suppress the wrinkles formation. On the contrary, an high blank holder force increases the frictional force which tends to cause blank ruptures. Thus it is important to reduce the friction to achieve a successful deep drawing operation. Tamai et al. [6] tried to improve the formability of high strength steel parts in deep drawing by detaching the tools from the die cushion periodically from the sheet. It was found that the sheet was automatically re-lubricated when the tool was detached. Komatsu and Murakami [7] reported a case where wrinkling in deep drawing was prevented by applying the stepwise drawing motion on a servo press with a constant clamping force. Wrinkles were eliminated by applying a smaller (about 1/3) blank holder force than the conventional motion with the stepwise motion. A similar effect for preventing the occurrence of wrinkling by the pulsating internal pressure was reported for tubes hydroforming [8]. A sheet product, which ruptures with the conventional crank motion, is successfully formed by optimizing the slide motion of a servo press [9]. In this motion, the punch touches the sheet with a slow speed, and the slide movement is once reversed between the pre-forming stage of the top portion and the drawing stage of the rectangular portion.

Development process of servo press method is accelerated as the capacity of servo motor become bigger. In the future, it's expected as a great alternative plan to replace conventional press method in order to: improve product quality, increase productivity, maintain tools integrity, and reduce energy consumption. Motion control in servo press method has to be effectively optimized depending on the shape and material characteristics. However, in the industrial field, the motion controls relied on experience or intuition of most skilled workers, so the workers can't avoid many trials and errors to find the optimized motion law [10]. Chanhee et al. [11], [12] carried out experimental validations by applying the design variables suggested by the safe forming window for the multi-stage forming.

Wei et al. [13] performed numerical analyses with multi-objective genetic algorithm for optimizing BHF and draw beads to minimize fracture and wrinkling during deep drawing process, simultaneously.

In this paper, the authors report the attempt to develop a technique to optimize the servo press motion law having as reference to obtain the maximum process benefit.

Numerical methodology description

The activities carried out by the authors refer precisely to the development of a numerical methodology which allows to analyze the influence factors, for comparison with the degrees of freedom made available by the servo press, in terms of stroke profile management.

Specifically, the work carried out by the research group followed the following steps:

1. Development, implementation and simulation of a numerical plan applied to an industrial test case, considering the actually material used online a low carbon steel (DC04 steel sheets, commonly used in the automotive industry [14]);
2. Obtained results analysis;
3. Numerical data correlation;
4. Optimization model implementation;
5. Analysis and performance evaluation of the obtained results with the developed optimization model;

6. Definition and resolution of the optimization problem for two different blanks geometry;
7. Optimized model validation.

Development, implementation and simulation of a numerical plan applied to an industrial test case

The chosen reference test case is a component for automotive application, a wheel fender, shown in Figure 6(a) obtained through a Cx2 processing method (from a single blank it is possible to obtain two parts: the right and the left fenders). Based on the current industrial process, the FE model of numerical simulation was calibrated to the real model.

Finite element analysis (FEA) was used to understand the deformation behavior of a material during the forming process. In this paper, the commercial finite element code Radioss® was used to run explicit forming simulation. HyperForm® was used to create the finite element mesh, assign the boundary conditions and to build Radioss input deck for the analysis. The Punch, Die and the Blank Holder were created using rigid materials, while Yoshida-Uemori Material was used for Blank. For the forming analysis were used shell elements and to reduce the calculation time while maintaining accuracy, an adaptive meshing scheme was used. The FE model of the tooling and the blank size are shown in Figure 1 and Figure 2.

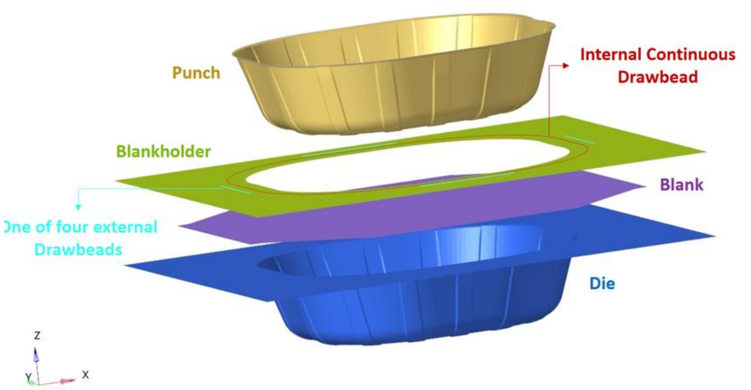

Figure 1 – FE Model created for simulation of the sheet forming process

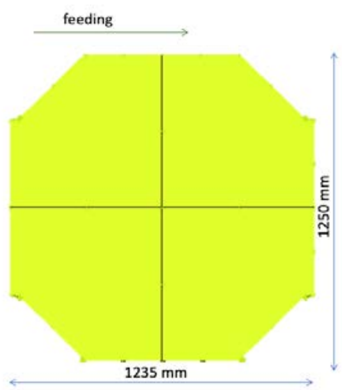

Figure 2 – Blank size

Table 1 reports sheet material properties used for blank and friction coefficient used in the simulation [15], [16]. The friction between the blank and the tool parts, was modelled by Coulomb's law.

Table 1- DC04 material properties and friction coefficient used in the simulation

σy [MPa]	Rm [MPa]	ν	h	B_0 [MPa]	C	m	b [MPa]	R_{sat} [MPa]	n	μ
130	500	0.3	0.526	168	657.9	1.281	8.980	558.6	0.19	0.125

In particular:

σy → Yield stress

Rm → ultimate stress

ν → Poisson's ratio

B_0 → Initial size of the bounding surface

h → Material parameter for controlling work hardening stagnation

C → Parameter for kinematic hardening rule of yield surface

m → Parameter for isotropic and kinematic hardening of the bounding surface

R_{sat} → Saturated value of the isotropic hardening stress

b → Center of the bounding surface

n → hardening coefficient

μ → Coulomb friction

The simulation of the traditional process refers to a constant punch speed equal to 2000 mm/s (this data set up is referred to the simulation context). This run has been indicated as RUN0 and represents the traditional drawing operation. The drawbeads have been numerically modeled as a geometric profile made by a line to which the analytical (friction) and geometric (shape) parameters are associated. Figure 3 and Figure 4 show the results related to the forming process simulation for RUN0. These outputs represent the basis for response extrapolation used for the analytical optimization model. Failure criteria used in the analysis was based on the Forming Limit Diagrams (FLD). Specifically, in Figure 3 FLD is shown, considering the initial blank with maximum dimensions equal to 1235 x 1250 mm and the blank nominal thickness equal to 0.77 mm.

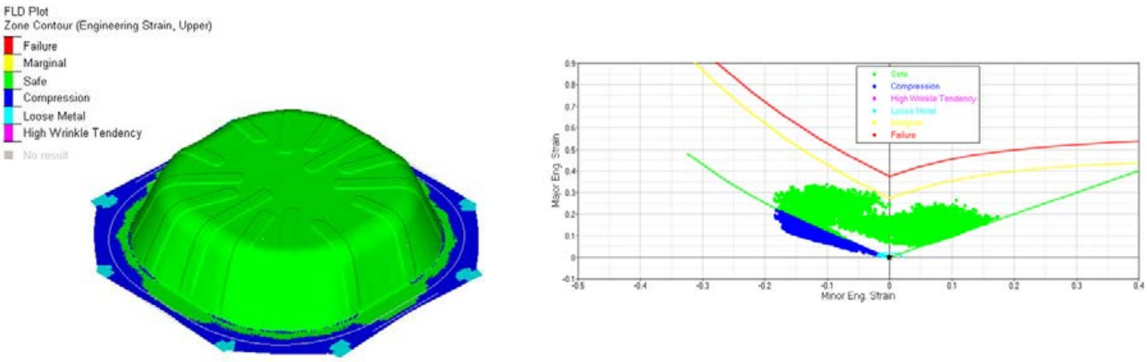

Figure 3 – FLD for RUN0

In Figure 4, instead, the percentage thinning map is shown. It is possible to observe how the maximum thinning, mainly in correspondence of the fillet radii and at the end of the stroke, is equal about to 25%.

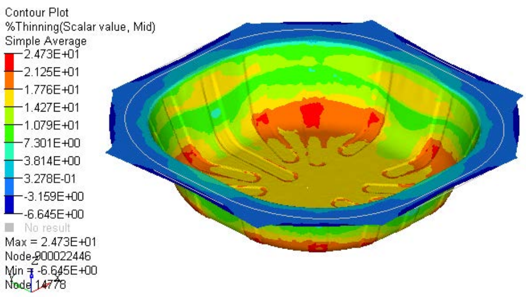

Figure 4 – Percentage thinning distribution for RUN0

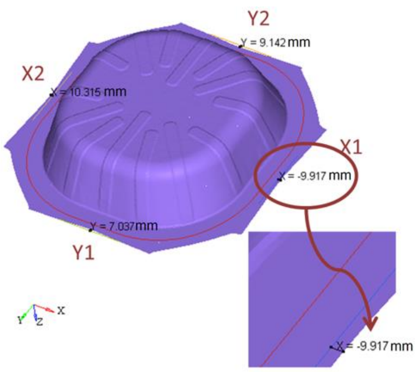

Figure 5 - Output variables definition X1, X2, Y1 and Y2 and related detail of X1

Table 2 - Output variables list

max thick [%]	min thick [%]	max Rforce DIE [N]	X1 [mm]	X2 [mm]	Y1 [mm]	Y2 [mm]
Output 1	Output 2	Output 3	Output 4	Output 5	Output 6	Output 7

Figure 6 shows the comparison between the product obtained by forming with a traditional mechanical press and the numerical model. Compared to what is usually evaluated in output, as maximum and minimum percentage thinning and maximum reaction forces, the model response has been also evaluated with respect to the formed material flow in the die, for industrial interest. Once the output variables X1, X2, Y1 and Y2 have been defined, the maximum distance of the linear edges of the blank has been reported from the first drawbead border (Figure 5). The output variables set is shown in Table 2.

Outputs 4, 5, 6 and 7 are considered negative if the blank exceeds the position of the drawbead with respect to which the measure is taken (in the sense of the formed material flow in the die), positive if, instead, the blank does not exceed the drawbead edge.

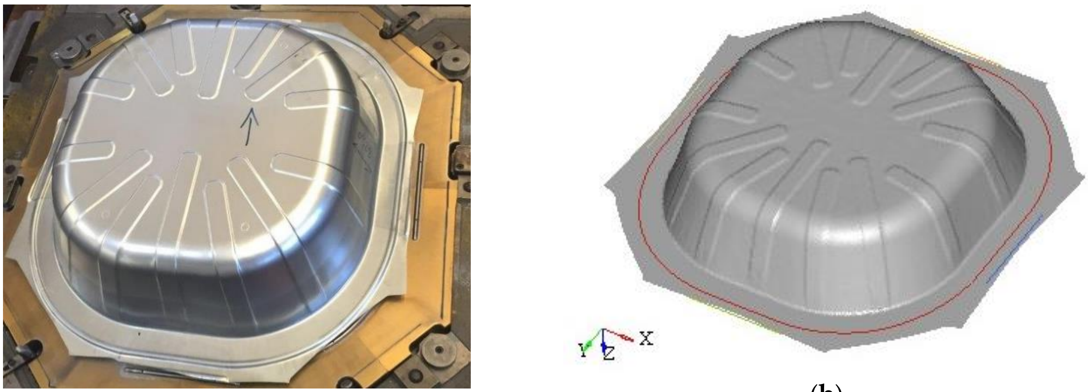

(**a**) (**b**)

Figure 6 - Comparison between: (**a**) the product obtained by forming with a traditional mechanical press and (**b**) the numerical model

The introduction of kinematic control with servo presses allows to better take advantage of the intrinsic characteristics of the material with respect to the deformation state. The material has a dependency by the strain rate, but it mainly has a dependency by the deformation state. In particular, the material changes its performance, based on the deformation history. This behaviour is the main feature that can be well used through a driven process with a servo press. Starting from these considerations, the authors have developed a procedure that has allowed to investigate precisely this behavior, introducing not only a change in the slide speed, but also a disengagement interval of the forming tool from the blank during forming. This type of slide stroke is called "stepwise", because the stroke of the slide has return steps of the slide itself.

The Figure 7 and the Figure 8 show a detail of the input variables for the definition of the experiment plan through which it is possible to identify the input variables of the defined simulation plan. For the specific case of interest only one disengagement has been considered.

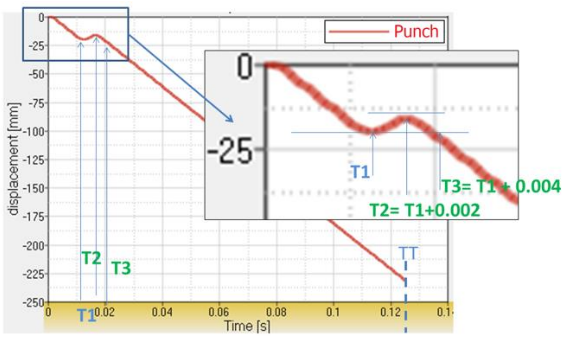

Figure 7 – Input timing definition on stepwise curve

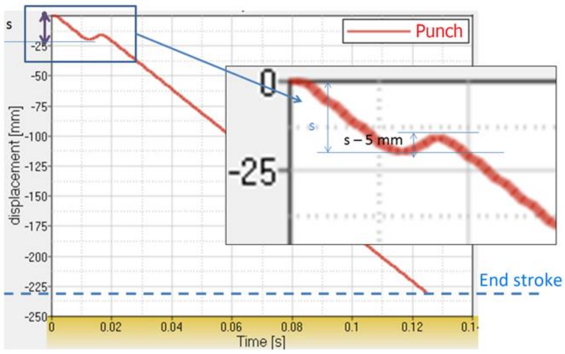

Figure 8 – Input stroke definition on stepwise curve

In particular, the input variables are:

- S → tool stroke point where the return takes place
- T1 → time at which the return occurs (speed inversion)
- T2 → return end time (velocity inversion) with position equal to S+5 mm
- T3 → return to S position
- TT → termination time, coinciding to a stroke equal to "end stroke".

In the case of RUN0, T1 coincides with TT, while S coincides with the total travel of the tool. For each of the identified input variables the following constraints have been defined:

- 50 mm < S < FF-10 mm
- 0.009 s < T1 < 0.01 s
- 0.046 s < TT < 0.233 s
- FF = 231 mm (fixed value)
- T2 = T1 + 0.002 s (value fixed by T1)
- T3 = T1 + 0.004 s (value fixed by T1).

Where FF is the end stroke, T2 and T3 are variables depending on T1. The runs, related to the defined experimental plan, characterized by the variables described above are reported in Table 3.

Table 3 - Design variables for experiment plan runs

Run#	S [mm]	T1 [s]	TT [s]	Run#	S [mm]	T1 [s]	TT [s]
1	50	0.0748	0.1874	14	162.64	0.0804	0.1681
2	99.28	0.0916	0.1729	15	155.6	0.0972	0.2068
3	211.92	0.0944	0.1439	16	183.76	0.0496	0.1148
4	57.04	0.0468	0.1826	17	141.52	0.1	0.139
5	226	0.0832	0.202	18	85.2	0.0636	0.1536
6	134.48	0.044	0.2165	19	64.08	0.0412	0.1342
7	197.84	0.0356	0.2116	20	190.8	0.0608	0.1923
8	78.16	0.086	0.1245	21	169.68	0.0776	0.1197
9	204.88	0.0384	0.1632	22	106.32	0.058	0.11
10	218.96	0.0664	0.1487	23	127.44	0.0328	0.1294
11	92.24	0.0888	0.2213	24	148.56	0.0524	0.1584
12	176.72	0.072	0.231	25	71.12	0.0552	0.2262
13	120.4	0.0692	0.1971	26	113.36	0.03	0.1778

Based on Table 3, for each input file, starting from RUN0, the tool displacement curve and the termination time of the simulation have been modified. The other two points of the curve included between T1 and TT are the points T2 and T3, where relative displacement S - 5 mm and again S, are automatically calculated. The plan described above relates to a single blank geometry (blank 0). In reality, to better evaluate the advantage respect to material savings, a second plan has been evaluated, identical to the first, but for a modified blank dimensions (blank 1). A size reduction, in the perpendicular direction to the blank feed, equal to 7.5 mm has been defined. This choice derives from the possibility of always being able to use the same tool for shearing, but with a smaller width coil. A blank of smaller dimensions is thus obtained without any change for the shearing tool.

Discussion of the obtained results

From the numerical analysis set up described above two simulation plans have been obtained. The results, for the outputs described in the Table 2, are reported below for the blank 0 (Table 4), and for the blank 1 in (Table 5).

Table 4 - Output of BLANK 0 simulation plan

RUN	max thick [%]	min thick [%]	max Rforce DIE [N]	X1 [mm]	X2 [mm]	Y1 [mm]	Y2 [mm]
1	20.2	-7.5	2.02E+06	0.632	-0.517	-16.984	-18.473
2	20.0	-7.3	1.92E+06	0.508	-0.048	-16.191	-18.851
3	22.1	-6.9	2.01E+06	5.97	5.691	-10.963	-12.754
4	19.3	-7.4	1.97E+06	-0.996	-0.523	-17.991	-19.98
5	22.1	-7.1	1.99E+06	5.058	5.365	-11.243	-13.195
6	21.0	-7	2.01E+06	3.536	3.576	-13.534	-15.507
7	25.3	-6.3	2.00E+06	14.672	14.819	-3.418	-5.069
8	23.1	-6.6	2.76E+06	9.776	9.201	-8.404	-10.098
9	25.0	-6.2	1.98E+06	14.01	14.455	-3.736	-5.168
10	22.6	-6.7	2.01E+06	6.975	7.556	-9.517	-11.036
11	20	-7.4	2.04E+06	-0.839	0.209	-18.533	-19.615
12	21.6	-7	2.02E+06	4.415	4.591	-12.61	-14.069
13	19.6	-7.3	1.98E+06	1.049	1.192	-15.7	-17.665
14	21.1	-7	1.93E+06	3.787	3.828	-13.306	-15.226
15	20.7	-7.2	1.89E+06	3.298	3.819	-13.848	-15.51
16	23.5	-6.7	1.20E+06	10.651	10.94	-6.804	-8.568
17	21.8	-6.9	2.00E+06	6.657	6.285	-10.66	-12.524
18	19.3	-7.4	2.13E+06	-0.483	0.4	-16.86	-18.779
19	19.7	-7.4	2.10E+06	-0.513	0.362	-16.986	-19.325
20	23.3	-6.9	1.20E+06	6.344	6.501	-10.528	-12.538
21	22.8	-6.9	1.98E+06	7.009	6.67	-10.403	-11.965
22	20.6	-7	1.87E+06	4.996	4.54	-12.106	-14.586
23	21.6	-7	1.89E+06	5.988	5.698	-11.908	-13.041
24	21.5	-7	2.05E+06	5.272	4.765	-12.078	-13.765
25	19.1	-7.4	-2.02E+06	-0.675	-0.919	-17.808	-19.328
26	20.3	-7.3	1.95E+06	2.953	2.545	-14.286	-16.651

The maximum thickness reduction is obtained in RUN7, while the maximum thickness increase value (wrinkles probability) is obtained in RUN1. The maximum and minimum reaction force values are obtained, respectively, for RUN8 and RUN16/20, while the maximum material recall in the die occurs for the RUN4, RUN11 and RUN25.

Table 5 - Output of BLANK 1 simulation plan

RUN	max thick [%]	min thick [%]	max Rforce DIE [N]	X1 [mm]	X2 [mm]	Y1 [mm]	Y2 [mm]
1	20.2	-7.5	1.84E+06	-8.1	-7.7	-15.3	-15.5
2	19.5	-7.6	1.96E+06	-4.7	-4.4	-18	-16.9

RUN	max thick [%]	min thick [%]	max Rforce DIE [N]	X1 [mm]	X2 [mm]	Y1 [mm]	Y2 [mm]
3	21.6	-7	1.98E+06	-2.1	-1.9	-11.2	-10.5
4	19.1	-7.3	1.87E+06	-6	-5.9	-18.9	-19.3
5	21.9	-7.3	2.37E+06	-1.9	-1.2	-11.2	-12.1
6	21.9	-8.2	2.05E+06	-7.5	-7.8	-25	-25.8
7	24	-7.5	2.17E+06	-2.9	-3.6	-15.7	-14.4
8	22.8	-6.6	1.88E+06	-3.4	-3.4	-4.4	-4.1
9	24.3	-7.2	2.18E+06	-7	-7.6	-12.3	-13.6
10	24.2	-7.7	2.06E+06	-2.5	-2.8	-17.5	-18.4
11	19.1	-7.5	1.94E+06	-8.5	-8.2	-20.3	-19.9
12	21.9	-7.2	2.04E+06	0.3	0.3	-13.6	-17.2
13	19.4	-7.4	1.86E+06	-5.8	-5.5	-16.8	-14.9
14	21.2	-7	2.00E+06	-2.7	-1.7	-14.2	-12.8
15	20.1	-7.3	2.09E+06	3.9	4.7	-15.7	-14.9
16	23.4	-7.5	2.08E+06	0.2	0.7	-17.5	18.5
17	22.3	-7	1.75E+06	0.5	0.6	-10.7	-9.9
18	19.8	-7.6	2.06E+06	-6	-5.7	-18.6	-17.2
19	21.2	-7.6	1.82E+06	-7.1	-6.9	-18.6	-17.3
20	22	-7.8	2.02E+06	-3.5	-3.4	-20	-20.6
21	22.7	-6.8	1.95E+06	1.4	1.5	-10	-9.5
22	21.9	-7.2	2.07E+06	-0.9	-0.5	-12.2	-11.8
23	21.2	-7.8	1.91E+06	0.7	1	-20.5	-21.4
24	20.9	-8.1	2.10E+06	-5.7	-5.7	-23.4	-24.9
25	19.1	-7.6	1.91E+06	-8.1	-7.9	-19.5	-18
26	19.3	-8.1	1.95E+06	-5	-4.9	-25	-26.4

For the plan relating to the blank 1, the maximum and minimum percentage of thinning values are obtained, respectively, for RUN9 and RUN6. The maximum and minimum reaction force values are obtained, respectively, for RUN5 and RUN17, while the maximum material recall in the die occurs for RUN1, RUN25 and RUN26. The results analysis shows that the blank dimension reduction has influence on the outputs. The results related to the geometric variable, must be analyzed considering the value of X1 and X2. For the two blanks they are always different because the blank size changes in X direction. It is therefore an output that cannot be considered in an absolute sense, but it is strongly dependent by the blank geometry. The post processing, of some of the simulations carried out for the simulation plan, is reported below. In particular, Figure 9 and Figure 10, show the percentage thinning distribution and X1, X2, Y1 and Y2 values for RUN20 and RUN22 for the blank0, while Figure 13 and Figure 14, the same output for the blank1 for RUN1 and RUN11 are reported.

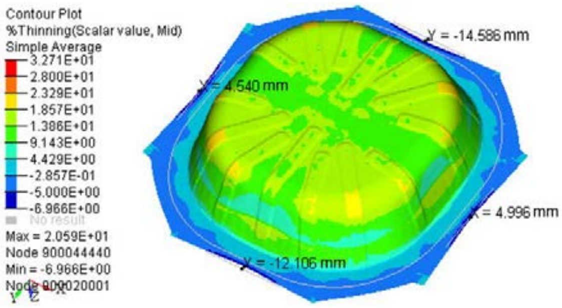

Figure 9 - Percentage thinning distribution and X1, X2, Y1 e Y2 values for the RUN22 – blank0

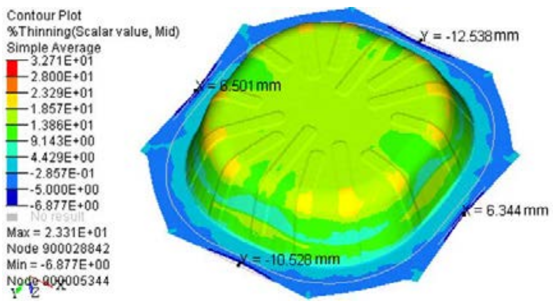

Figure 10 - Percentage thinning distribution and X1, X2, Y1 e Y2 values for the RUN20 – blank0

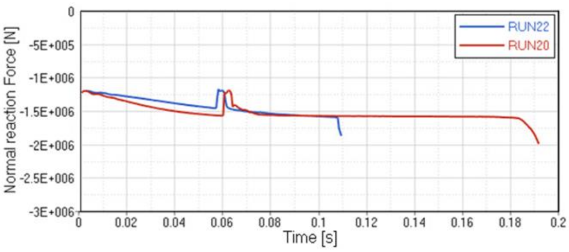

Figure 11 - Reaction force curves comparison between RUN20 and RUN22 – blank0

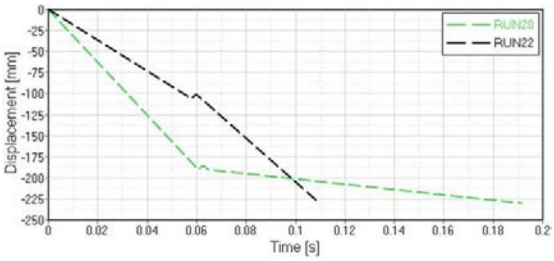

Figure 12 - Punch displacement with stepwise, in correspondence of S and T1. TT represents the last point of the curve with maximum value in x axis – blank0

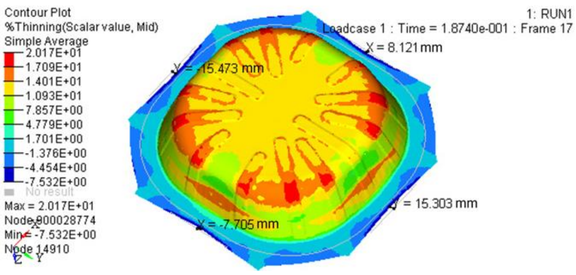

Figure 13 – Percentage thinning distribution and X1, X2, Y1 e Y2 values for the RUN1 – blank1

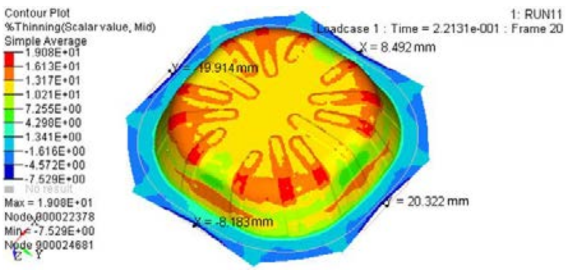

Figure 14 - Percentage thinning distribution and X1, X2, Y1 e Y2 values for the RUN11 – blank1

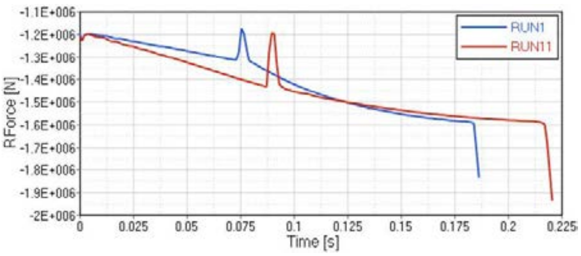

Figure 15 – Reaction force curves comparison between RUN1 and RUN11 – blank1

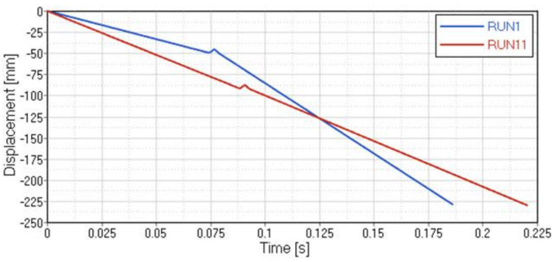

Figure 16 – Punch displacement with stepwise, in correspondence of S and T1. TT represents the last point of the curve with maximum value in x axis – blank1

For all the highlighted runs it is evident how, when a stepwise happens it is possible to detect a reaction force reduction (Figure 11, Figure 12, Figure 15 and Figure 16).

The output values X1, X2, Y1 and Y2 are considered negative if they exceed the drawbead profile (on the 4 sides) in the recall direction of material in the die. They will be positive only in the case of material excess compared to the drawbead profile. All four of the above cases present a slope variation of the reaction force in the coining phase. Furthermore, all considered cases report possible feasibility conditions, because the maximum thinning value, indicated as critical for material rupture equal to 28%, is never exceeded.

Optimization model implementation

Starting from the obtained results, shown in Table 4 and Table 5 , it has been possible to proceed with the implementation of the optimization model. The model has been investigated for all the output variables that have been identified and divided into two phase, in the first one the blank shape has been considered as an input variable, defined as “complete plan”, and in the second that instead analyzes two separate and distinct plans, defined as “semiplans”, one for each blank (blank0 and blank1), than the blank is not considered as input variable. The complete plan is reported in the present paper. In particular, an optimization procedure has been developed thanks to the integration of the optimization tool Dassault Systèmes ISight with Altair Radioss® solver. The reduction of the maximum reaction force has been chosen as objective function of the optimization phase. The optimal set up in terms of process variables definition has been investigated using Multi-Island Genetic Algorithm (MIGA) optimization algorithm.

Main effect analysis for complete plan

The descriptive graphics of the main effect (Main Effect Plot, MEP) have been used to examine the differences between the average levels of the response of interest, for one or more factors (process variables). There is a “main effect” when different levels of a factor influence the response differently. A Main Effect Plot represents, for each level of the considered factors, the response averages connected by a line. These graphs provide indications on the factors that have the greatest influence on the process responses variability. For the maximum thickness percentage reduction (max thick% output), the MEP (Figure 17) shows how the blank size does not have the same influence as it appears to be in the case of TT, T and S. This consideration is evident from how much the outputs deviate from the average value. In the particular case of the S variable, there is a growing response trend with respect to the max thick% output. The effect on the minimum thickness percentage reduction (min thick%) output variable is, on the other hand, less evident than the maximum percentage reduction (max thick%), the graph in Figure 18 shows, in fact, values very close to the average. Also the slope of the values obtained for the blank size variable is always relative to an interval very close to the average value. Regarding the output on the reaction force, instead, there is a low influence of all the input variables, if some points are excluded (anomalies) it can be seen (Figure 19) that the responses are very close to the average value. The possible changes of the blank geometry have particularly effect on the X1and X2 outputs value.

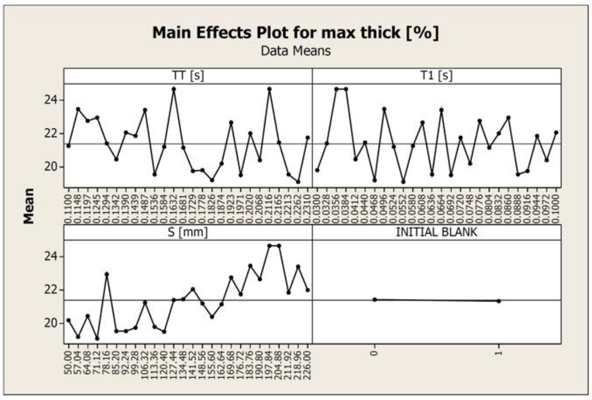

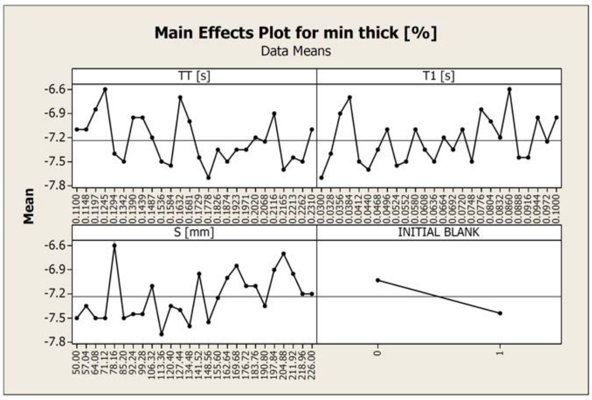

Figure 17 - MEP for max thick % output **Figure 18** - MEP for min thick % output

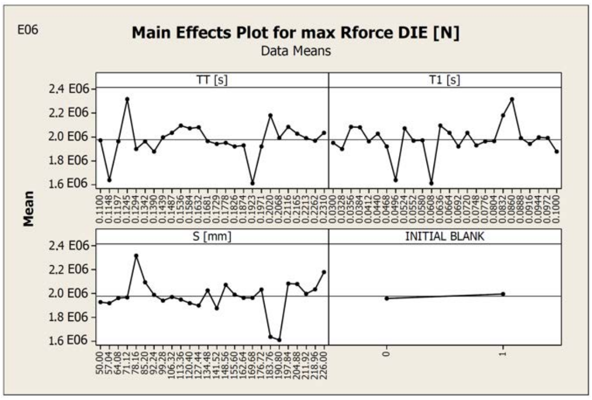

Figure 19 - MEP for reaction force output

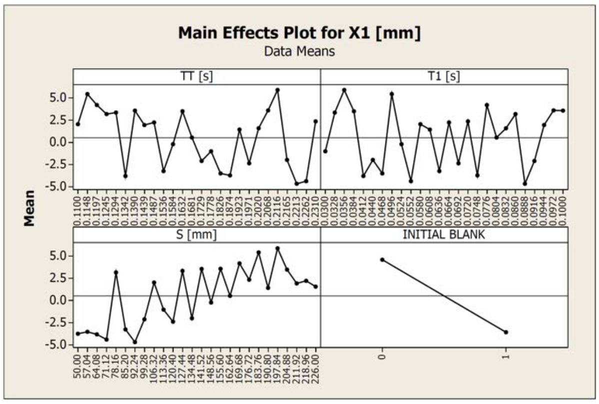

Figure 20 - MEP for X1 output

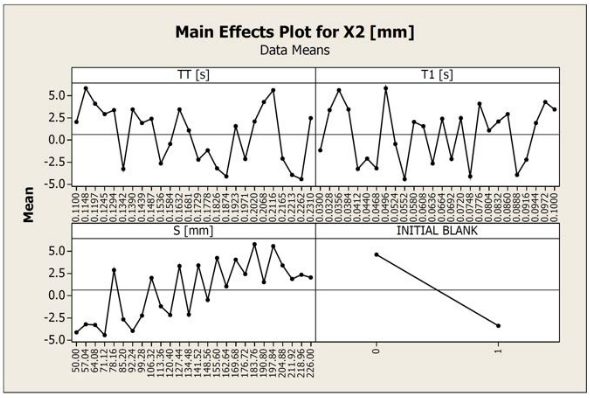

Figure 21 - MEP for X2 output

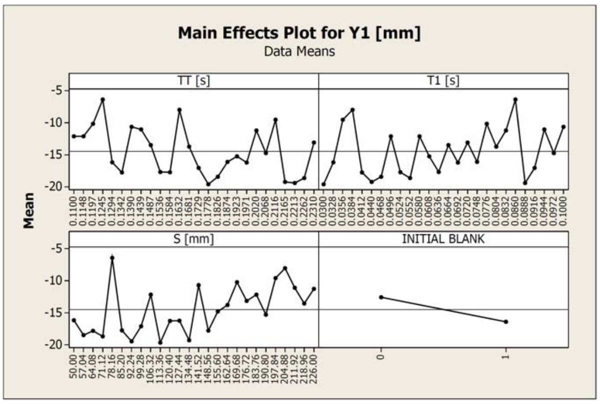

Figure 22 - MEP for Y1 output

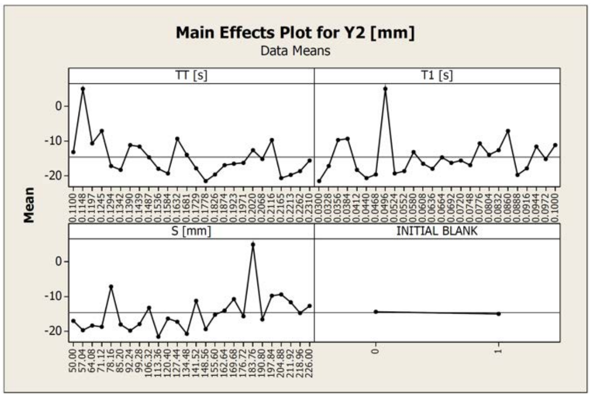

Figure 23 - MEP for Y2 output

As shown in Figure 20 and Figure 21, the identified input variables show a considerable influence on the responses values represented in these MEP and, in particular, the blank size one strongly influences these outputs.

Regarding the outputs Y1 and Y2, as shown in Figure 22 and Figure 23, the identified input variables (TT, T1 and S) show an influence on the output values while the blank size effect is drastically reduced. The Y dimension is not altered in the transition between the blank0 and blank1.

From the previous graphs, it can be seen that, in general, the TT, T1 and S parameters significantly influence the response variability with respect to its average value. The blank size variable, on the other hand, does not have a significant influence on the considered response variability.

Definition and resolution of the optimization problem for Blank0

In this specific case, three process parameters have been taken into consideration as possible variables: tool stroke S (mm), speed inversion time T1 (s) and termination time TT (s).

The optimization problem has been defined as follows:

Objective Function:	*Min (max_Rforce_Die)*	
Design Variables:	*50 mm ≤ S ≤ 226 mm*	
	0.03 s ≤ T1 ≤ 0.1 s	
	0.11 s ≤ TT ≤ 0.231 s	
Constraints:	*19% ≤ max_thick ≤ 28%*	*-8% ≤ min_thick ≤ -5%*

The design space constraints have been assigned by the maximum and minimum values of percentage reductions referring to numerical values.

In this case, with the assigned constraints, the solution of the optimization problem has been found for the combination:

S = 192.95 mm T1 = 0.0454 s TT = 0.11 s

Table 6 shows the numerical and regression models values correlation, for blank0 plan, and relative error evaluation. Compared to the original plan, an additional line has been added to show the run values for which it is possible to reach the feasibility limit for the output on the maximum percentage thinning.

In this case, with the assigned constraints, the solution of the optimization problem has been found for the combination:

S = 192.95 mm T1 = 0.0454 s TT = 0.11 s

Table 6 - Numerical and regression model values correlation - blank0 plan

RUN	INPUT			REGRESSION MODEL OUTPUTS			NUMERICAL OUTPUTS			ERRORS		
	S [mm]	T1 [s]	TT [s]	max thick [%]	min thick [%]	max Rforce DIE [N]	max thick [%]	min thick [%]	max Rforce DIE [N]	max thick [%]	min thick [%]	max Rforce DIE [N]
1	50.00	0.0748	0.1874	20.02	-7.34	2093295	20.20	-7.50	2022870	-0.91	-2.10	3.48
2	99.28	0.0916	0.1729	20.78	-7.17	2182846	20.00	-7.30	1918110	3.92	-1.83	13.80
3	211.92	0.0944	0.1439	22.11	-6.92	1993481	22.10	-6.90	2013660	0.04	0.30	-1.00
4	57.04	0.0468	0.1826	18.80	-7.58	1892017	19.30	-7.40	1968800	-2.60	2.48	-3.90
5	226.00	0.0832	0.2020	22.40	-6.99	2063007	22.10	-7.10	1989740	1.35	-1.57	3.68
6	134.48	0.0440	0.2165	21.22	-7.05	1897945	21.00	-7.00	2008330	1.05	0.65	-5.50
7	197.84	0.0356	0.2116	25.47	-6.19	2109164	25.30	-6.30	1999097	0.65	-1.76	5.51
8	78.16	0.0860	0.1245	22.47	-6.78	2547603	23.10	-6.60	2755880	0.31	1.22	-6.73
9	204.88	0.0384	0.1632	24.86	-6.29	1936617	25.00	-6.20	1982690	-0.55	1.41	-2.32
10	218.96	0.0664	0.1487	23.37	-6.65	2011086	22.60	-6.70	2008650	3.43	-0.68	0.12
11	92.24	0.0888	0.2213	20.00	-7.29	2081651	20.00	-7.40	2039430	0.00	-1.43	2.07
12	176.72	0.0720	0.2310	21.56	-7.07	2061384	21.60	-7.00	2023390	-0.17	0.94	1.88
13	120.40	0.0692	0.1971	19.88	-7.37	1888758	19.60	-7.30	1981650	1.44	0.99	-4.69
14	162.64	0.0804	0.1681	20.83	-7.20	1915638	21.10	-7.00	1927210	-1.27	2.79	-0.60
15	155.60	0.0972	0.2068	20.32	-7.31	1696835	20.70	-7.20	1893290	-1.85	1.51	-10.38
16	183.76	0.0496	0.1148	23.38	-6.51	1556814	23.50	-6.70	1200260	4.85	-5.71	-17.74
17	141.52	0.1000	0.1390	21.95	-6.89	2071463	21.80	-6.90	2001060	0.70	-0.20	3.52
18	85.20	0.0636	0.1536	20.00	-7.34	2177074	19.30	-7.40	2130240	3.60	-0.81	2.20
19	64.08	0.0412	0.1342	19.57	-7.41	2086636	19.70	-7.40	2100820	-0.67	0.16	-0.68
20	190.80	0.0608	0.1923	22.36	-6.90	1770676	23.30	-6.90	1200110	0.29	0.02	-11.90
21	169.68	0.0776	0.1197	22.20	-6.81	1906247	22.80	-6.90	1977980	-2.62	-1.34	-3.63
22	106.32	0.0580	0.1100	21.37	-6.97	1899818	20.60	-7.00	1873870	3.74	-0.39	1.38
23	127.44	0.0328	0.1294	21.40	-6.94	1947060	21.60	-7.00	1889500	-0.93	-0.84	3.05
24	148.56	0.0524	0.1584	21.15	-7.08	1807338	21.50	-7.00	2045660	-1.63	1.15	-11.65
25	71.12	0.0552	0.2262	19.18	-7.44	2027902	19.10	-7.40	2024410	0.39	0.59	0.17
26	113.36	0.0300	0.1778	20.59	-7.15	2059791	20.30	-7.30	1952500	1.45	-2.04	5.50
MIN	50.00	0.030	0.11	18.80	-7.58	1556814	19.10	-7.50	1200110	-2.62	-5.71	-17.74
MAX	226.00	0.10	0.23	25.47	-6.19	2547603	25.30	-6.20	2755880	4.85	2.79	13.80

The expected results of the model are reported in Table 7.

Table 7 - Optimal combination of regression model – Blank0

S [mm]	T1 [s]	TT [s]	Max_Rforce_DIE [N]	Max_thick [%]	Min_thick [%]	Objective and Penalty	Objective Function [N]	Penalty Function
182.847974	0.0454548	0.11000185	1472516	20	-6.42	1472516	1472516	0

The Pearson correlation or linear correlation (a measure of the strength of the association between the two variables) is calculated as follows for the X and Y parameters:

$$r_{xy} = \frac{\sum_{k=1}^{N}(x_k-\bar{x})(y_k-\bar{y})}{\sqrt{\sum_{k=1}^{N}(x_k-\bar{x})^2}\sqrt{\sum_{k=1}^{N}(y_k-\bar{y})^2}} \quad (1)$$

Where:

- k is a sample size
- x_k, y_k are the individual sample points indexed with k
- $\bar{x} = \frac{1}{n}\sum_{k=1}^{n} x_k \quad \bar{y} = \frac{1}{n}\sum_{k=1}^{n} y_k$

The "r" values will be within the range between -1 and 1, where the first value represents a perfect inverse linear correlation, the second a perfect direct linear correlation. The values close to zero and zero itself are indicative of a poor parameters correlation. Figure 24 shows the linear correlation matrix for the blank0 plan.

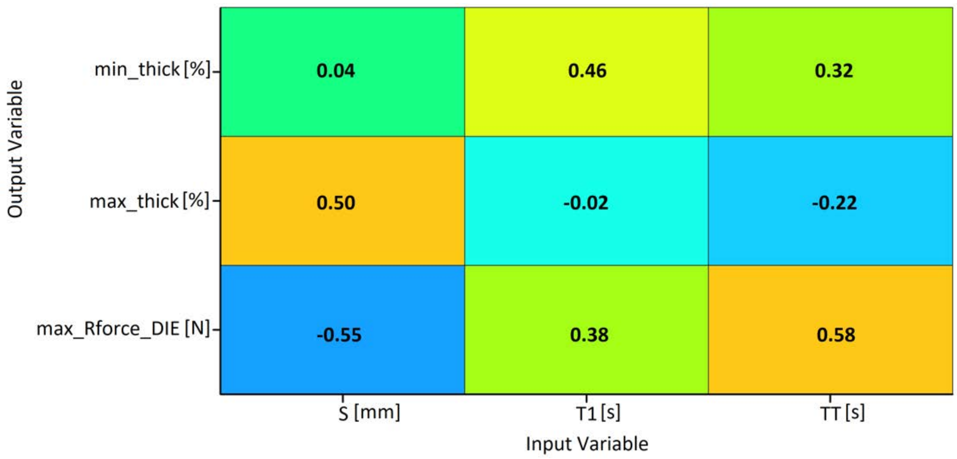

Figure 24 - Linear correlation matrix for the blank 0 plan

Figure 24 shows no correlation between the space before the motion inversion (S) and the minimum percentage thinning. Same result between the time on the first motion inversion (T1) and the maximum percentage thinning. Instead, the maximum reaction force and the process end time (TT) have a very strong direct correlation, the space S and the maximum reaction force are, instead, inversely correlated.

Figure 25 shows a history related to the research for the solution by the algorithm: the red dots correspond to solutions do not able to satisfy the given constraints, the black dots the ones able to satisfy them, and the green dots (located in X and Y with the fuchsia axes) represents the optimal solution in the explored design space.

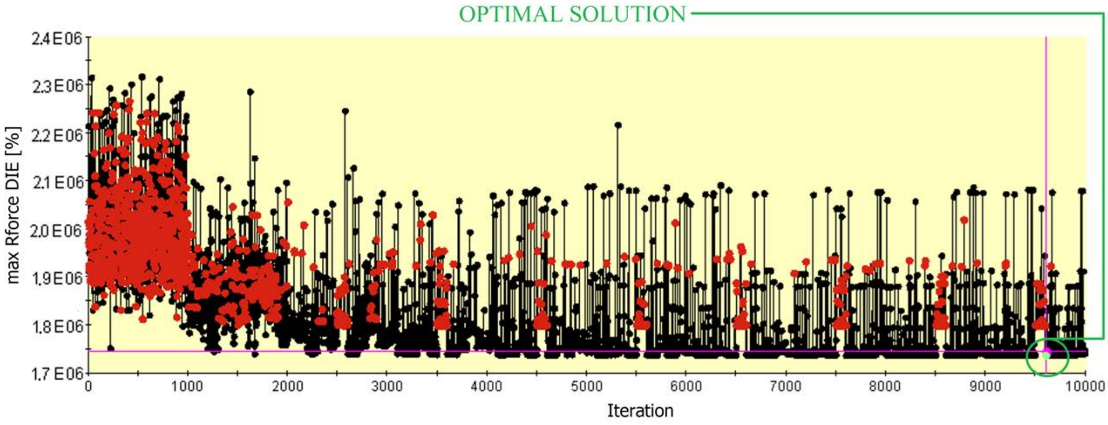

Figure 25 - Design explored with MIGA, blank0 plan

Definition and resolution of the optimization problem for Blank1

As in the case of blank0, below is reported the optimization problem definition for the model blank1 plan. The optimization problem has been defined as follows:

Objective Function:	*Min (max_Rforce_Die)*	
Design Variables:	*50 mm ≤ S ≤ 226 mm*	
	0.03 s ≤ T1 ≤ 0.1 s	
	0.11 s ≤ TT ≤ 0.231 s	
Constraints:	*19% ≤ max_thick ≤ 25%*	*-9% ≤ min_thick ≤ -6%*

The design space constraints have been assigned by the maximum and minimum values of percentage reductions referring to numerical values. Table 8 shows the numerical and regression model values correlation, for blank1 plan, and relative error. Compared to the original plan, an additional line has been added to show the run values for which it is possible to reach the feasibility limit for the output on the maximum percentage thinning.

Table 8 - Numerical and regression model values correlation – blank1 plan

RUN	INPUT			REGRESSION MODEL OUTPUTS			NUMERICAL OUTPUTS			ERRORS		
	S [mm]	T1 [s]	TT [s]	max thick [%]	min thick [%]	max Rforce DIE [N]	max thick [%]	min thick [%]	max Rforce DIE [N]	max thick [%]	min thick [%]	max Rforce DIE [N]
1	50.00	0.0748	0.1874	19.80	-7.42	1834375.021	20.20	-7.50	1835260	-1.96	-1.07	-0.05
2	99.28	0.0916	0.1729	20.12	-7.49	1937125.107	19.50	-7.60	1964070	3.17	-1.51	-1.37
3	211.92	0.0944	0.1439	22.17	-7.02	1972896.543	21.60	-7.00	1981810	2.66	0.23	-0.45
4	57.04	0.0468	0.1826	19.05	-7.58	1867188.059	19.10	-7.30	1871000	-0.25	3.82	-0.20
5	226.00	0.0832	0.2020	22.41	-7.27	2311269.029	21.90	-7.30	2371100	2.32	-0.47	-2.52
6	134.48	0.0440	0.2165	20.84	-7.61	2019189.077	21.90	-8.20	2045330	-4.84	-7.16	-1.28
7	197.84	0.0356	0.2116	24.39	-7.57	2158267.881	24.00	-7.50	2168100	1.62	0.92	-0.45
8	78.16	0.0860	0.1245	22.79	-6.72	1880775.054	22.80	-6.60	1877480	-0.05	1.86	0.18
9	204.88	0.0384	0.1632	23.84	-8.09	2138040.466	24.30	-7.20	2178410	-1.91	12.37	-1.85
10	218.96	0.0664	0.1487	23.37	-7.60	2146448.837	24.20	-7.70	2060450	-3.41	-1.26	4.17
11	92.24	0.0888	0.2213	19.26	-7.45	1965398.706	19.10	-7.50	1939120	0.83	-0.60	1.36
12	176.72	0.0720	0.2310	21.55	-7.28	2057738.866	21.90	-7.20	2044910	-1.61	1.05	0.63
13	120.40	0.0692	0.1971	19.69	-7.71	2028697.012	19.40	-7.40	1858140	1.47	4.17	9.18
14	162.64	0.0804	0.1681	20.66	-7.56	1956293.479	21.20	-7.00	2001820	-2.52	7.94	-2.27
15	155.60	0.0972	0.2068	19.58	-7.31	2022827.292	20.10	-7.30	2089730	-2.59	0.19	-3.20
16	183.76	0.0496	0.1148	23.54	-7.52	2057717.659	23.40	-7.50	2076100	0.62	0.32	-0.89
17	141.52	0.1000	0.1390	21.55	-6.69	1841041.399	22.30	-7.00	1753830	-3.38	-0.62	4.97
18	85.20	0.0636	0.1536	20.29	-7.66	1942531.283	19.80	-7.60	2058790	2.50	0.78	-5.65
19	64.08	0.0412	0.1342	20.31	-7.48	1895316.719	21.20	-7.60	1824710	-4.18	-1.62	3.87
20	190.80	0.0608	0.1923	22.08	-7.70	2140322.430	22.00	-7.80	2020780	0.38	-1.34	5.92
21	169.68	0.0776	0.1197	22.72	-6.94	1910920.430	22.70	-6.80	1949350	0.09	2.11	-1.97
22	106.32	0.0580	0.1100	22.36	-6.99	2048391.365	21.90	-7.20	2069810	2.11	-2.91	-1.03
23	127.44	0.0328	0.1294	21.23	-8.02	1960883.548	21.20	-7.80	1908440	0.12	2.85	2.75
24	148.56	0.0524	0.1584	20.99	-7.96	1997574.579	20.90	-8.10	2098800	0.45	-1.78	-4.82
25	71.12	0.0552	0.2262	19.27	-7.45	1880469.975	19.10	-7.60	1911420	0.88	-1.97	-1.62
26	113.36	0.0300	0.1778	19.96	-7.91	1935405.070	19.30	-8.10	1948510	3.40	-2.32	-0.67
MIN	50.00	0.030	0.11	19.05	-8.09	1834375.021	19.10	-8.20	1753830	-4.84	-7.16	-5.65
MAX	226.00	0.10	0.23	24.39	-6.69	2311269.029	24.30	-6.60	2371100	3.40	12.37	9.18

In this case, with the assigned constraints, the solution of the optimization problem has been for the combination:

S = 64.24 mm *T1 = 0.0318 s* *TT = 0.131 s*

The expected results of the model are reported in Table 9.

Table 9 - Optimal combination of regression model – Blank1

S [mm]	T1 [s]	TT [s]	Max_Rforce_DIE [N]	Max_thick [%]	Min_thick [%]	Objective and Penalty	Objective Function [N]	Penalty Function
64.23899	0.031864	0.131	1863534.957	20	-7.43	1863534.957	1863534.957	0

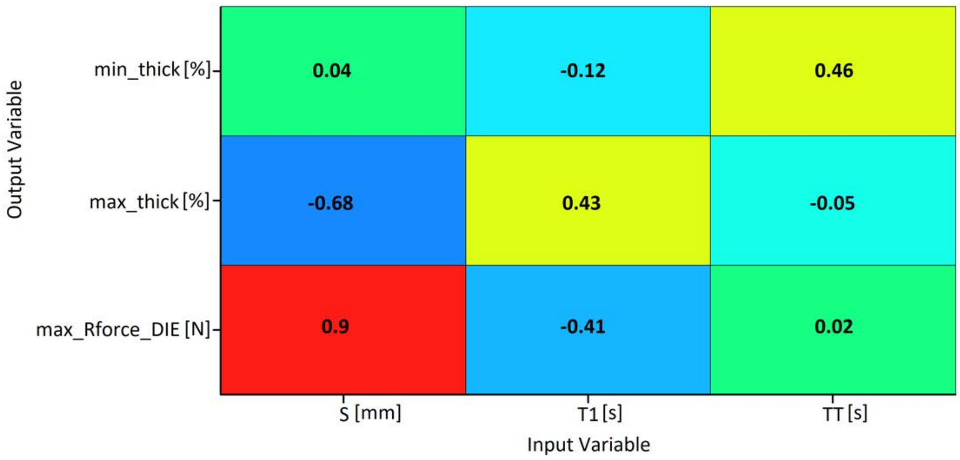

Figure 26 - Linear correlation matrix, blank 0

From the correlation matrix shown in Figure 26 it can be seen that output *max_Rforce_DIE* and *max_thick* do not depend on the end of process times (TT), in the same way the *min_thick* does not depend on S. Instead, *max_Rforce_DIE* and the space S are directly related, the latter is inversely related to *max_thick*. The search history of the solution is reported in Figure 27.

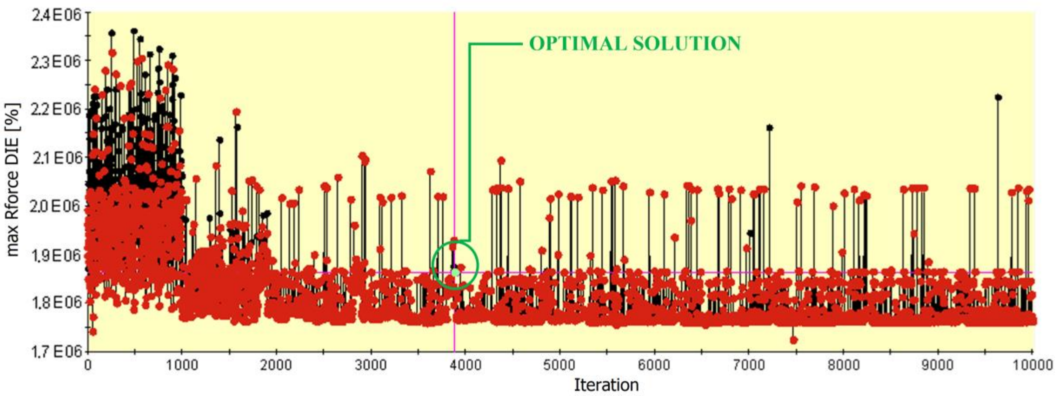

Figure 27 - Design explored with MIGA, blank1 plan

Model validation

In order to test the optimization model reliability, numerical analysis runs have been performed for the combinations as reported in Table 7 and Table 9, in accordance with parameters combination relating to the optimal solution suggested by the optimization procedure. The punch displacement input curve definition is reported, for the two "optimal runs", in Figure 28. The results for the two runs are shown below, in particular, in Figure 29 is reported the trend of die reaction force curves, both for the case blank0 and blank1. It is evident how, when a stepwise happens it is possible to detect a reaction force reduction (Figure 28 and Figure 29). For both cases there is a slope variation of the reaction force in the coining phase.

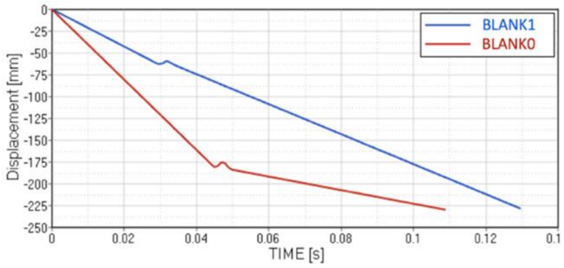

Figure 28 – Displacement vs time comparison for the optimal combination (according to the regression model) for blank0 and blank1 plan

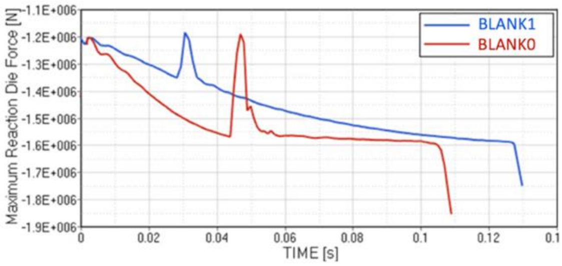

Figure 29 – Die reaction force comparison for both simulation plan

Figure 30 and Figure 31 report the percentage thinning distribution (max and min) and X1, X2, Y1 e Y2 output for optimal combination relative to the blank0 and blank1.

Thinning percentage distribution shows very low values for the Blank1, while it remains similar for the runs performed with the plan for the Blank0. This result shows, in addition, that the blank reduction involves a thinning reduction, as well as a scrap reduction, without compromise the obtaining of the final geometry of the part. The output values X1, X2, Y1 and Y2 are all negative because they exceed the drawbead profile (on the 4 sides) in the recall direction of material in the die.

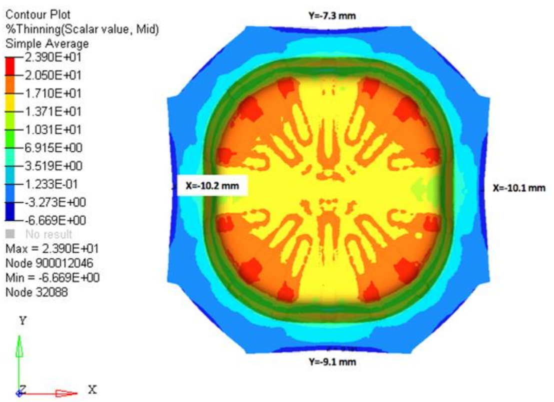

Figure 30 - Percentage thinning distribution and X1, X2, Y1 e Y2 for optimal combination relative to the blank0

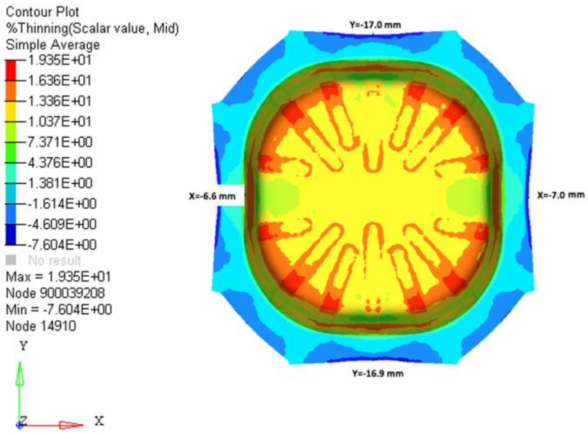

Figure 31 - Percentage thinning distribution and X1, X2, Y1 e Y2 for optimal combination relative to the blank1

Table 10 reports the output for the optimal models (blank0 and blank1).

Table 10 - Output for optimal model: blank0 (optimal0) and blank 1 (optimal1)

RUN	max thick [%]	min thick [%]	max Rforce DIE [kN]	X1 [mm]	X2 [mm]	Y1 [mm]	Y2 [mm]
Optimal0	23.9	-6.7	1855	-10.2	-10.1	-9.1	-7.3
Optimal1	19.3	-7.6	1751	-6.6	-7.0	-16.9	-17.0

To evaluate the model performance, in Table 11 the percentage error calculation of numerical results respect to regression model results is reported.

Table 11 - Percentage error calculation of numerical results vs regression model results

RUN	max thick error [%]	min thick error [%]	max Rforce DIE error [kN]
Optimal0	-19.5%	4.4 %	-26 %
Optimal1	3.2 %	2.3 %	6.0%

As It can be seen from Table 10 and Table 11, the model for blank1 conditions appears more reliable than the model obtained for blank0 ones.

Conclusions

The reported research activity demonstrates how it is possible to support the servo press adoption in industrial contexts with appropriate innovative optimization procedures in order to maximize the positive effect given by their application. In fact, the proposed optimization procedure allows the manufacturing engineers to explore the best servo press configurations for any given process combination in terms of: material, thickness and geometry of the formed component. The obtained results have given the perception of the effectiveness of the proposed approach. Anyway the authors have to proceed with specific research activities to increase the robustness of the proposed methodologies. In fact, it is important to consolidate what has been developed in connection to a useful correlation with experimental activity in which several process combinations are investigated (material, initial thickness, geometry of the formed component) in order to evaluate the influence of the possible combination on the reliability of the proposed approach. Another element of development it is represented by the possible adoption of different optimization algorithms in order to evaluate the optimization results sensitivity to the proposed optimization strategy.

References

1. Ando H., Application of Servo System in Recent Press Machines. *Journal of the Japan Society for Technology of Plasticity*, **2004**, 45(526):877–882. (in Japanese).
2. *Japan Machinery Federation, Japan Forming Machinery Association* (**2005**). Standardization of Servo-Motor Drive Press Machines (in Japanese).
3. Altan T., Groseclose A., Servo-Drive Presses–Recent Developments, 10, (**2009**). Umformtechnisches Kolloqium Darmstadt.
4. Osakada K., Application of Servo Presses to Metal Forming Processes. *Steel Research International, Supplement Metal Forming* **2010**, vol. 81, no. 9, 9–16.
5. Amada Co., Ltd. HP: http://www.amada.co.jp/english/.
6. Tamai Y., Yamasaki Y., Yoshitake A., Imura T., Improvement of Formability in Stamping of Steel Sheets by Motion Control of Servo Press. *Steel Research International, Supplement Metal Forming* **2010**, vol. 81, no. 9, 686–689.
7. Komatsu I., Murakami T. *Practical Use of Servo Press*, (**2009**). The Nikkan Kogyo Shimbun, Ltd. pp. 48–49 (in Japanese).
8. Mori K., Maeno T., Maki S., Mechanism of Improvement of Formability in Pulsating Hydro Forming of Tubes. *International Journal of Machine Tools and Manufacture*, (**2007**), 47(6):978–984.
9. Nakano T., Press Machine Trends and Servo Press Forming Examples, *Steel Research International, Supplement Metal Forming* **2010**, vol. 81, no. 9, 682–685.
10. Jun-Ku L., Hyun-Cheol K., The Optimization of Servo Press Method for Sheet Metal Forming. *13th International LS-DYNA Users Conference*, **2014**.
11. Chanhee W., Dongjin Kim, Jonghun Yoon, Minimizing wrinkling formation of GPa-grade steels in multi-stage crash forming process. *The International Journal of Advanced Manufacturing Technology*, ***2019.***

12. Wei L., Yuying Y., Multi-objective optimization of sheet metal forming process using Pareto-based genetic algorithm. *J. Mater Process Technol,* 208:499–506, **2008**.
13. Meng B., Wan M., Wu X., Yuan S., Xu X., Liu J., Inner wrinkling control in hydrodynamic deep drawing of an irregular surface part using drawbeads. *Chin J Aeronaut, 27:697–707,* **2014.**
14. Tomasz T., Hirpa G. Lemu, Effect of Computational Parameters on Springback Prediction by Numerical Simulation. *Metals* **2017**, 7, 380; doi:10.3390/met7090380.
15. Zang S. L., Thuillier S., Le Port A., Manach P. Y., Prediction of anysotropy and hardening for metallic sheet in tension, simple shear and biaxial tension, *International Journal of Mechanical Science* 53 (**2011**) pp. 338-347.
16. Radioss Reference Guide, **2017.**